

# Single-Electron Counting Statistics with a Finite Frequency Bandwidth

Narii Watase, Masayuki Hashisaka and Toshimasa Fujisawa

Department of Physics, Tokyo Institute of Technology, 2-12-1-H81, Ookayama, Meguro, Tokyo, 152-8851, Japan

## Abstract

Single-electron counting statistics, which provide deep insight in correlated electron transport, can also be influenced by measurement apparatus such as finite frequency bandwidth of a charge detector. We have developed an analysis technique to obtain actual tunneling rates through a quantum dot when the detector has a limited bandwidth. The correction performance is confirmed by simulating the filtering effect on single-electron counting scheme, which is effective even when tunneling rates are close to the upper edge of the bandwidth.

## 1. Introduction

Charge detection of a quantum dot (QD) by using a quantum point contact (QPC) is widely used to study single electron dynamics in nanostructures [1]. Every single electron tunneling events can be detected in real time, and the statistical analysis of the time-domain data allows us to evaluate the followings; tunneling rates through the barriers, correlated electron tunneling with non-Poissonian characteristics, and spin-dependent tunneling with spin-charge conversions, for example[2-5]. In practice the QPC current has to be analyzed with a limited frequency bandwidth to eliminate unwanted noise. However, this bandwidth inevitably removes some tunneling events, and thus the obtained statistics or tunneling rates of the measured events can be different from those of the true events. In this work, we have analytically investigated the statistics of tunneling events through a QD with a single energy state when the detector has a limited bandwidth, and derived a simple correction scheme to estimate the actual tunneling rates.

## 2. Detectable statistics with finite bandwidth

We consider a single QD coupled to a QPC detector as shown in Fig. 1(a). With a large bias voltage  $V_{QD}$ , single-electron transport is supposed to be unidirectional from the left to the right with tunneling rates  $\Gamma_{in}$  and  $\Gamma_{out}$ . As shown in Fig. 1(b), the QPC detector current  $I_D(t)$  fluctuates between high and low levels corresponding to empty and occupied states in the QD. This current is converted into a voltage  $V_D(t)$  with an I-V converter and appropriate filters. Here we assume that the overall response function is expressed as a standard first-order low-pass filter characterized by a time constant  $\tau_f$ . The voltage waveform  $V_D(t)$  would be somewhat distorted like in Fig. 1(c). This waveform  $V_D(t)$  is digitized into two values with a threshold voltage  $V_{th}$ . Typically  $V_{th}$  is set at the middle of the two voltages,  $V_{D,H}$  and  $V_{D,L}$ , respectively for the empty and occupied states, or can be hysteretic depending on the previ-

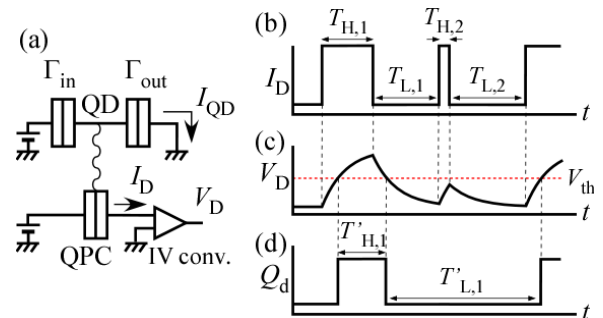


Fig. 1. (a) Schematic diagram of charge detection measurement of single-electron tunneling events through a quantum dot. (b) Typical detector QPC current  $I_D(t)$  with dwell times  $T_{H,i}$  and  $T_{L,i}$ . (c) Amplified voltage  $V_D(t)$  and the threshold voltage  $V_{th}$ . (d) Digitized data  $Q_d(t)$  with measured dwell times  $T'_{H,i}$  and  $T'_{L,i}$ .

ous state. Typical response time  $\tau_{th}$  from an transition event to reaching this threshold is given by  $\tau_{th} = -\tau_f \ln \eta$  with a threshold factor  $\eta = V_{th}/(V_{D,H} - V_{D,L})$ , which is typically  $\eta = 1/2$ . The digitized data, shown in Fig. 1(d), is regarded as the dot charge  $Q_d(t)$ .

However, as one can see in the comparison of Figs. 1(b) and 1(d), the obtained dwell times  $T'_{H,i}$  and  $T'_{L,i}$  are not identical to the true dwell times  $T_{H,i}$  and  $T_{L,i}$ . Hereafter, primed variables are used for quantities with finite bandwidth. The first dwell time  $T'_{H,1}$  in the figure is slightly different from the true one  $T_{H,1}$ , but this difference is negligibly small ( $\tau_f \ln 2$  in the worst case). Serious errors come from undetected events like the second dwell time  $T_{H,2}$  in Fig. 1(b), which is missing in Fig. 1(d). Importantly, the original two low-level dwell times  $T_{L,1}$  and  $T_{L,2}$  are misinterpreted as a single dwell time  $T'_{L,1}$ , which can alter the distribution of the dwell time. In the following, we show how the finite bandwidth influences the measurable statistics, and provide a simple way to correct the errors.

We consider the incoming and outgoing tunneling process to be Poisson. Namely, the true dwell time  $T_{H/L}$  is distributed with the probability  $P_{H/L}(T_{H/L}) = \frac{1}{\tau_{H/L}} e^{-T_{H/L}/\tau_{H/L}}$ , which has mean  $m_{H/L}$  and standard deviation  $\sigma_{H/L}$  identical to the tunneling time constant  $\tau_{H/L}$ , i.e.  $m_{H/L} = \sigma_{H/L} = \tau_{H/L}$ . The first-order low-pass filter removes events with short dwell time less than  $\tau_{th}$ . Corresponding undetected probability is expressed as  $(1 - \beta_{H/L})$  with  $\beta_{H/L} = e^{-\tau_{th}/\tau_{H/L}}$ . First we consider the case where undetected events exist only for the high level; finite  $\beta_H$  but  $\beta_L = 0$  corresponding to  $\tau_L \gg \tau_H \sim \tau_f$ . When the measurement gives a dwell time  $T'_L$ , there might be  $n$  hidden undetected events with short dwell time  $T_{H,i}$  ( $i = 1 \dots n$ ) in the period  $T'_L$ . Here, actual dwell time  $T_{L,i}$  ( $i = 0 \dots n$ ) are constrained with the observation ( $T'_L = \sum_{i=0}^n T_{L,i}$ ). The probability of having  $n$  hidden events is

$p(n) = (1 - \beta_H)^n \beta_H$ . Corresponding distribution function of  $T'_L$  composed on  $(n+1)$  low-level dwell times  $T_{L,i}$  reads

$$P'_L(T'_L) = \int_0^\infty P_L(T_{L,0}) dT_{L,0} \int_0^\infty P_L(T_{L,n}) dT_{L,n} \delta\left(T'_L - \sum_{i=0}^n T_{L,i}\right), \quad (1)$$

where dwell times of the hidden events,  $T_{H,i}$ , are ignored. The overall distribution function is found to be

$$P'_L(T'_L) = \sum_{n=0}^\infty p(n) P_L^{(n)}(T'_L) = \frac{\beta_H}{\tau_L} e^{-\beta_H T'_L / \tau_L}. \quad (2)$$

It has the same form as the original  $P_L(T_L)$  but with a longer characteristic time  $\tau'_L = \tau_L / \beta_H$  by the factor  $\beta_H (< 1)$ . The above formula can be used to obtain the true tunneling rate  $\Gamma_{\text{out}} = \tau_L^{-1} = (\tau'_L \beta_H)^{-1}$  from the measured  $\tau'_L$ .

In practice, undetected errors can occur in both levels, which mak the microscopic analysis difficult. Nevertheless, we apply the above formula for both levels for simplicity. Then measured time constants  $\tau'_H$  and  $\tau'_L$  would be given by

$$\tau'_L = \tau_L e^{-\tau_{\text{th}} / \tau_H}, \quad \tau'_H = \tau_H e^{\tau_{\text{th}} / \tau_L}. \quad (3)$$

Conversely, one can obtain true tunneling rates  $\Gamma_{\text{in}} = \tau_H^{-1}$  and  $\Gamma_{\text{out}} = \tau_L^{-1}$  by solving the non-linear coupled equations Eq. 3 from the measurement outcome  $\tau'_H$  and  $\tau'_L$ .

### 3. Numerical simulations of stochastic process

To demonstrate the validity of the above analytical estimate, we performed numerical simulation of Poisson random processes. Random telegraph signal generated with the time constants  $\tau_H$  and  $\tau_L$  is distorted by the first-order filter with a time constant  $\tau_f$ . The distorted waveform  $V_D(t)$  is digitized into two values with the hysteretic threshold ( $\eta = 1/4$ ). Distributions of the dwell times  $T'_H$  and  $T'_L$  are evaluated by making their histograms.

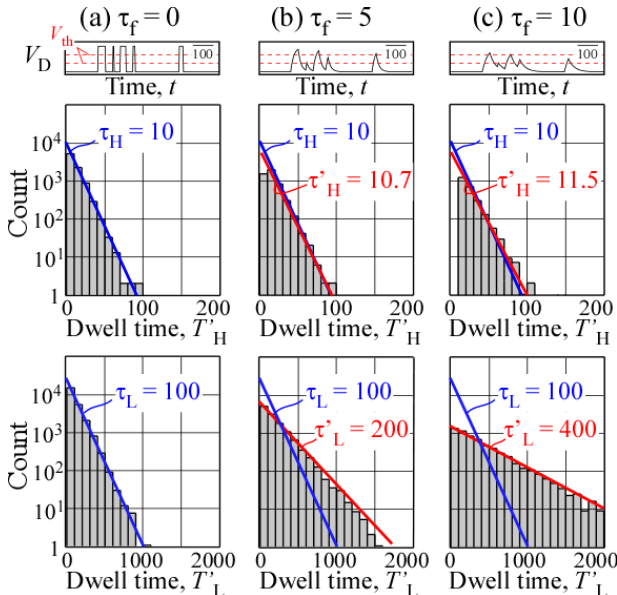


Fig. 2. Numerical simulation of counting statistics for asymmetric tunneling barriers ( $\tau_H = 10$  and  $\tau_L = 100$ ). All time scales are in an arbitrary unit. (a) No filtering and (b) filtering with  $\tau_f = 5$ , and (c) with  $\tau_f = 10$ . Filtered waveforms (solid lines) and hysteretic threshold levels (dashed lines) are shown in the top panels. Histograms for high and low levels are shown in the middle and bottom panels. The distributions agree well with the analytical solutions (red lines).

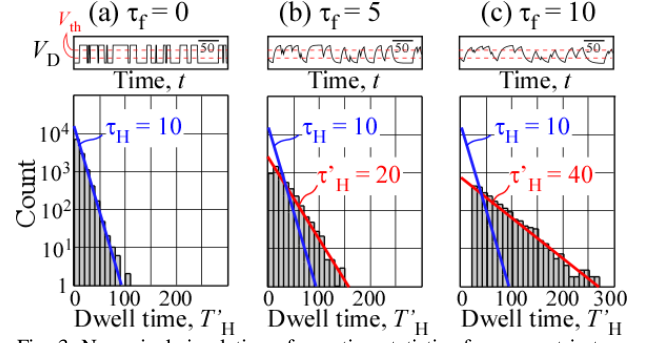


Fig. 3. Numerical simulation of counting statistics for symmetric tunneling barriers ( $\tau_H = \tau_L = 10$ ). (a) No filtering, and (b) filtering with  $\tau_f = 5$ , and (c) with  $\tau_f = 10$ .

Figure 2 shows typical results for asymmetric tunneling time-constants  $\tau_H = 10$  and  $\tau_L = 100$  in an arbitrary unit. As seen in  $V_D(t)$  traces in the top panels, the signal is distorted in (b) for  $\tau_f = 5$  and (c) for  $\tau_f = 10$  as compared to the no-filtering case in (a) for  $\tau_f = 0$ . Corresponding histograms for  $T'_H$  and  $T'_L$  are shown respectively in the middle and bottom panels. They are deviated from the true distribution functions (blue lines labeled by  $\tau_H$  and  $\tau_L$ ). Events for dwell time less than  $\tau_f$  are missing, as seen in the middle panel of Fig. 2(c). Histograms of  $T'_L$  shows a completely different slope  $\tau'_L$ , four times as large as  $\tau_L$ , in the bottom panel. It should be noted that they are well reproduced by the analytical formula  $P'_L(T'_L)$  multiplied by a reasonable factor (red lines labeled by  $\tau'_H$  and  $\tau'_L$ ).

Figure 3 shows the results for symmetric case of  $\tau_H = \tau_L = 10$ , where  $V_D(t)$  traces and histograms  $T'_H$  are shown. Undetected events at  $T'_H < \tau_{\text{th}}$  and large time-constant  $\tau'_H > \tau_H$  are clearly seen in Fig. 3(c). Importantly, the distribution is well reproduced with the solution of Eq. (3). This ensures that Eq. 3 can be used even when tunneling events for both high and low levels are partially undetectable ( $\tau_H, \tau_L \sim \tau_f$ ). The top trace in Fig. 3(c) represents the waveform at  $\tau_H = \tau_L = \tau_f$ , which almost deviates from two-level telegraph signal. The correction with Eq. (3) is effective to obtain true time constants (tunneling rates) even in such situation.

### 4. Summary

Practical and useful scheme to obtain true tunneling rates is provided for a single-electron counting statistics with a finite frequency bandwidth.

### Acknowledgements

We thank M. Yamagishi and K. Muraki for supporting single-electron counting experiments, which have motivated us to consider the problem described in this abstract.

### References

- [1] M. Field et al., Phys. Rev. Lett. **70**, 1311 (1993).
- [2] L. S. Levitov, H. Lee, G. B. Lesovik, J. Math. Phys. **37**, 4845 (1996).
- [3] S. Gustavsson et al., Phys. Rev. Lett. **96**, 076605 (2006).
- [4] T. Fujisawa, T. Hayashi, R. Tomita, and Y. Hirayama, Science **312**, 1634 (2006).
- [5] J.R. Petta et al., Science **309**, 2180 (2005).